Analysis of Propulsion Methods for Long-Range AUVs

AUTHORS

Daniel Steinberg
Asher Bender
Ariell Friedman
Michael Jakuba
Oscar Pizarro
Stefan Williams
Australian Centre for Field Robotics, School of Aerospace Mechanical and Mechatronic Engineering, University of Sydney

ABSTRACT

Underwater gliders use a buoyancy engine and symmetric wings to produce lift. During operation, gliders follow a saw-tooth trajectory, making them useful vehicles for profiling ocean chemistry. By operating at low speeds with low hotel loads, gliders achieve a high endurance. Man-portable, propeller-driven autonomous underwater vehicles (AUVs) are capable of level flight and can also follow terrain to yield high-quality benthic imagery. These platforms typically operate at high speeds with high hotel loads resulting in relatively low endurance. Although both vehicles are used to collect oceanographic data, constraints on how these vehicles are used differentiate the nature of data they collect. This article examines whether one method of propulsion can provide an intrinsic advantage in terms of horizontal range at low speed, regardless of sampling design. We employ first-principle analysis that concludes that either class of vehicle can be designed to achieve the same horizontal transit performance regardless of speed. This result implies that the choice of propulsion method should be driven exclusively by the application and operational requirements.

Keywords: AUV Propulsion, Long-range transit, Autonomous Underwater Vehicles, Underwater gliders, Transit efficiency

1. Introduction

Autonomous underwater vehicles (AUVs) are increasingly being used to replace more labor intensive methods of collecting data from the ocean. AUVs also enable entirely untended surveys, where no support vessel is required during a mission. Since these platforms do not require *in situ* human intervention during mission execution, their running costs are low compared to the cost of deployment and recovery. Untended surveys are most economic when the number of deployments is minimized, which can be achieved by maximizing the achievable range of the AUV. The purpose of this article is to uncover whether buoyancy-driven modes of propulsion are intrinsically more or less efficient at maximizing achievable horizontal range than propeller-driven modes of propulsion, with all else being equal.

The success of underwater gliders in monitoring programs requiring frequent deployments (Schofield et al., 2008) suggests that man-portable AUVs are an amenable size for monitoring roles from a budgetary and handling perspective (Griffiths et al., 2001). The REMUS100 AUV and the Slocum glider are similarly sized man-portable AUVs and will be used as a point of reference in this analysis.

The REMUS100 is a man-portable, propeller-driven AUV designed for seafloor imaging and water-column survey in energetic environments. At its nominal speed of 1.5 m/s, the total energy consumption of REMUS100 is O(10 W) and results in an endurance of 22 h (REMUS100 specification).

The Slocum glider is comparable in size to REMUS100, but it has been designed for taking oceanographic profiles. To attain long range, the Slocum was designed to travel at a low speed (0.4 m/s), with a low hotel load, O(1W) (Electric glider, Davis et al., 2002). Despite storing only slightly more than twice the energy of REMUS100 (REMUS100 specification; Davis et al., 2002), Slocum can achieve considerably longer ranges and has a typical endurance of 30 days.

The difference in endurance between REMUS100 and Slocum is due to the way the vehicles are operated. The effect of hotel load and horizontal velocity on range is given by Furlong et al. (2007):

$$R = \frac{E}{P_{\mathrm{P}} + P_{\mathrm{H}}} \cdot \dot{x}$$

where E is the on-board energy storage, P_{P} and P_{H} are the propulsive and hotel powers, respectively, and $\dot{x}$ is the horizontal velocity. If the efficiency of the propulsion system (η), the density

of the fluid (ρ) and the vehicle drag (C_{DS}) based on a reference area (S) are known, the propulsive power can be written as a function of velocity:

$$P_P = \frac{\rho \dot{x}^3 S C_{DS}}{2\eta}.$$

Furlong et al. (2007) showed that given these parameters, maximum range can be obtained by differentiating range with respect to propulsive power. The optimal velocity for a given hotel power is then given by

$$\dot{x} = \sqrt[3]{\frac{\eta P_H}{\rho S C_{DS}}} \quad (1)$$

Equation 1 shows that it is optimal to operate at a relatively high velocity for a high hotel load and a relatively low velocity for low hotel loads. This relationship governs the difference in endurance between REMUS100 and Slocum. The REMUS100 must be operated at a high velocity so that sufficient survey coverage is obtained before its hotel load exhausts energy reserves. On the other hand, the relatively low hotel load of Slocum allows it to be operated at low velocities.

For a given hull design and hotel load, a vehicle's range can be maximized by operating at a velocity that satisfies Equation 1. For the remainder of this article, we assume a low power hotel load and focus on the efficiency of propulsion methods at low velocities. In particular, we will determine if there are any compelling reasons to pick a propeller over gliding (or vice versa) for a low velocity transit.

The rest of this article builds on Steinberg et al. (2009) and is organized as follows. A metric for evaluating achievable range per unit of energy, transit performance, is proposed in Section 2. The transit performance of a propeller-driven AUV and glider are derived in Section 3. These first-principle models are compared in Section 4. For the purpose of relating this general result to realistic designs, we have used the REMUS100 AUV and the Slocum glider as examples. Based on this outcome, Section 5 concludes that the choice of propulsion method should be driven primarily by the application and operational requirements of the vehicle.

2. The Transit Performance Metric

The purpose of this study is to determine the efficiency of gliders and propeller-driven AUVs as they move between two sampling locations. Hence, transit performance will be measured by how many *horizontal* meters these vehicles can travel per Joule of energy (m/J). This metric is a variant of net transport economy defined by Jenkins et al. (2003).

Two cases are considered:

1. A propeller-driven AUV
2. A buoyancy-driven autonomous underwater glider

The transit performance measure, Λ, is equivalent to the reciprocal of the horizontal component of the AUVs propulsive force, i.e.

$$\text{Energy} = \text{Force} \times \text{Distance}$$

so

$$\frac{\text{Distance}}{\text{Energy}} = \frac{1}{\text{Force}}$$

or

$$\Lambda(m/J) = \frac{1}{T_{\text{horiz}}(N)}$$

The transit performance of an AUV with a loss-less propulsion system is derived in Section 3.1. Its purpose is to normalize away the inverse quadratic dependence of transit performance on velocity, which is a result of drag and common to all underwater vehicles. We term this normalized quantity transit efficiency, which takes the following form:

$$\lambda_{\text{Vehicle}} = \frac{\Lambda_{\text{Vehicle}}}{\Lambda_{\text{Ideal}}}.$$

It is important to note that this form of efficiency only accounts for losses due to the mode of propulsion with respect to an ideal propulsion model. As a result, this efficiency metric is not a multiplicative loss that can be used in deriving the total efficiency of a system. Additional losses in the drive chain, such as mechanical and electrical losses, are *not* included in this definition of efficiency.

The following general assumptions are used for this analysis:

1. All vehicles compared have an equivalent hull design and hull drag coefficient. Volume devoted to energy stores, propulsion, and control hardware is the same in each AUV. Furthermore, the hotel and sensing loads are equivalent as the mission requirements are the same.
2. Any non-steady accelerating motions are assumed to occupy a negligibly small fraction of the total mission time, hence only steady motions are considered for the purpose of this analysis. Consequently, straight-line transit is assumed, i.e. no turning motions are considered.
3. The propeller-driven and ideal AUVs are neutrally buoyant, and seawater has a constant density.

Propeller-driven AUVs are usually slightly positively buoyant as a fail-safe.

To overcome their buoyancy and local variations in seawater density, these AUVs make use of control surfaces or actuators. Normally, this would introduce additional drag due to lift from the hull and control surfaces at non-zero angles of attack (Furlong et al., 2007). In our analysis, we ignore this effect and assume neutral buoyancy. Neutral buoyancy could be achieved by installing a small buoyancy control system on the vehicle.

The assumptions made in this analysis omit mechanical and electrical losses incurred between the energy source and the final propulsive power. The mechanisms for delivering energy from the source to propulsion are different for propeller and buoyancy-driven AUVs. For example, a propeller-driven AUV will lose energy at a constant rate through losses in the power electronics, couplings, and bearings of the drive system. Prior to design improvements in 2000, REMUS100 had a brushed DC motor which operated at an estimated 65% efficiency at 80 W (Allen et al., 2000). Since then, REMUS100 has been equipped with a brushless DC motor and a magnetic torque transfer. This new design uses a more efficient motor and eliminates a rotating shaft seal. An efficiency measure is not quoted for these changes but it is likely to increase efficiency to 70-80%.

The primary energy losses in a glider are due to the buoyancy engine. Instead of a constant drain on the energy source, buoyancy engines demand high current loads when the buoyancy engine is actuated at the glider's inflexion points. On Slocum, the efficiency of the buoyancy engine based on electrical energy delivered to the pump including energy loss in the battery is approximately 50% (Griffiths et al., 2007). The amount of energy that can be extracted from batteries will vary with battery chemistry and the way they are used. Some batteries are better able to handle the high peak loads of buoyancy engines and others are better suited to the constant drain of propeller-driven AUVs (Bradley et al., 2001).

FIGURE 1

Free body diagram of an AUV with loss-less propulsion.

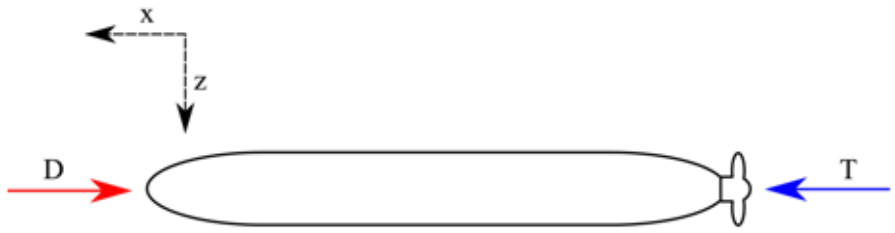

While these figures are important in determining the over efficiency of the vehicles, they are beyond the scope of our first-principles analysis. Our transit efficiency metric will not reflect overall system efficiencies because we are only concerned with transit performance relative to an ideal case, and no other losses. The analysis presented in this article produces an upper bound on efficiency for the propulsion modes presented.

3. Transit Performance

In this section, the transit performance metrics are derived from first principles for propeller-driven AUVs and gliders. Using these models, we aim to uncover any velocity dependence that would indicate that one method of propulsion is superior to the other for low speed transit. We show that neither of the models are dependent on velocity.

3.1. Ideal Propulsion

An AUV with a loss-less propulsion system will have perfect transit efficiency for the selected hull shape. This vehicle is presented to normalize the transit performance of the propeller-driven AUV and glider.

From Figure 1, it can be seen that for a steady horizontal velocity, thrust must equal drag

$$T = \frac{1}{2}\rho S_h \dot{x}^2 C_{Dh} \tag{2}$$

where S_h is the AUV hull frontal area, C_{Dh} is the AUV's drag coefficient referenced to S_h, and ρ is the fluid density. Hence

$$\Lambda_{Ideal} = \frac{1}{T} = \frac{2}{\rho S_h \dot{x}^2 C_{Dh}} \tag{3}$$

3.2. Propeller-Driven AUV

Momentum theory can be used to model the performance of a propeller. Although momentum theory does not account for fluid rotation in the slipstream or energy lost to viscous drag, it is an attractive model because propeller geometry can be expressed with one design parameter. The ideal propulsive efficiency of an actuator disk λ_{AD}, predicted by momentum theory (Carlton, 2007), is given by

$$\lambda_{AD} = \frac{2}{1 + \left(\frac{2T}{\rho S_p \dot{x}^2} + 1\right)^{\frac{1}{2}}}$$

where S_p is the area of the actuator disk. Since the thrust, T, produced by the actuator disk must overcome hull drag

(Equation 2), the efficiency of the propeller-driven AUV can be restated as

$$\lambda_{AD} = \frac{2}{1 + \left(C_{Dh} f_p^{-2} + 1\right)^{\frac{1}{2}}} \tag{4}$$

where the propeller–hull ratio, $f_p = d_p/d_h$, defines the ratio between the actuator disk diameter, d_p, and the hull diameter, d_h.

Since the energy supplied to an actuator disk is reduced by the efficiency of the actuator disk, the transit performance for the propeller-driven AUV can be written as

$$\Lambda_{AD} = \frac{\lambda_{AD}}{T}$$

If transit performance is normalized by the ideal propulsion scheme (Equation 3), the transit efficiency of the propeller-driven AUV is simply the efficiency of the actuator disk (Equation 4)

$$\frac{\Lambda_{AD}}{\Lambda_{Ideal}} = \lambda_{AD}$$

Under the simplifying assumptions of this section, for a given hull design the transit efficiency of a propeller-driven AUV is only a function of the propeller–hull ratio. An outcome of this result is that transit efficiency is independent of horizontal velocity.

3.3. Glider/Buoyancy-Driven AUV

A typical glider configuration uses a buoyancy engine and symmetric wings to translate buoyancy into lift to induce horizontal motion. Figure 2 shows the forces acting on the glider in the longitudinal plane.

FIGURE 2

Free body diagram of the forces acting on a glider in the longitudinal plane.

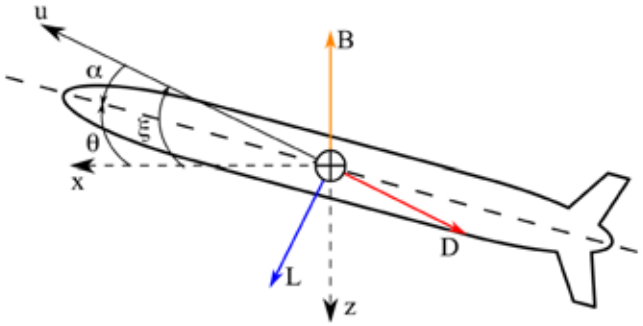

Only the longitudinal plane of motion is considered in the transit performance model, so it is necessary to resolve the lift and total drag forces to the horizontal (x) axis. Using Figure 2, the horizontal forces can be determined from $\sum F_x = 0$

$$0 = L\sin\xi - D\cos\xi$$
$$L\sin\xi = D\cos\xi$$

Here, ξ is the glide-path angle and $L \sin \xi$ and $D \sin \xi$ are equivalent to the horizontal propulsive force. Transit performance is given by their inverse

$$\Lambda_G = \frac{1}{L\sin\xi} = \frac{1}{D\cos\xi} \tag{5}$$

Drag, D, and lift, L, are given by Roskam (2008) and Sherman et al. (2001)

$$D = \frac{1}{2}\rho u^2\left(S_h C_{Dh} + S_w C_{DLw}\alpha^2\right) \tag{6}$$

$$L = \frac{1}{2}\rho u^2 S_w C_{Lw}\alpha \tag{7}$$

Here C_{Lw} is the wing lift coefficient referenced to wing planform area, S_w. Velocity along the glide path is u, α is the angle of attack, and C_{DLw} is the wing drag-due-to-lift or induced drag. For simplicity, we have excluded body lift and induced drag.

Drag in Equation 6 is composed of parasitic and lift-induced components. The expression for lift in Equation 7 is analytically simpler. Since either can be made to arrive at transit performance in Equation 5, we proceed by substituting for L

$$\Lambda_G = \frac{2}{\rho u^2 S_w C_{Lw}\alpha\sin\xi} \tag{8}$$

An equation for angle of attack is derived by Graver (2005). To reduce the dimensionality of this equation, we assume that there is no parasitic wing drag ($C_{Dw} = 0$), so angle of attack becomes

$$\alpha = \frac{\frac{1}{2}\rho S_w C_{Lw}}{\rho S_w C_{DLw}} \tan\xi \left(-1 + \sqrt{1 - 4\frac{\frac{1}{2}\rho S_w C_{DLw}}{\left(\frac{1}{2}\rho S_w C_{Lw}\right)^2}\left(\frac{1}{2}\rho S_h C_{Dh}\right)\cot^2\xi} \right)$$

$$= \frac{C_{Lw}}{2C_{DLw}} \tan\xi \left(-1 + \sqrt{1 - 4\frac{C_{DLw}C_{Dh}}{C_{Lw}^2} \cdot \frac{S_h}{S_w}\cot^2\xi} \right)$$

Wing drag-due-to-lift, C_{DLw}, is a function of the wing lift coefficient, C_{Lw}, when these coefficients use wing planform area as their common reference area (Roskam, 2008)

$$C_{DLw} = \frac{C_{Lw}^2}{\pi A e}$$

here A is the wing aspect ratio, and e is the wing's span efficiency factor. So substituting for C_{DLw} and assuming the wing geometry perfectly utilizes the lift distribution along the wing ($e = 1$), angle of attack becomes

$$\alpha = \frac{\pi A}{2C_{Lw}} \tan\xi \left(-1 + \sqrt{1 - 4\frac{C_{Dh}S_h}{\pi S_w A}\cot^2\xi} \right)$$

From Figure 2, we have defined $\xi = \theta + \alpha$, however Graver (2005) defines $\xi = \theta - \alpha$. To use α in these models, its sign has to be reversed. So the angle of attack for our model is

$$\alpha = \frac{\pi A}{2C_{Lw}} \tan\xi \left(1 - \sqrt{1 - C_{Dh} f_b^{-2}\cot^2\xi} \right) \tag{9}$$

where we have substituted

$$4\frac{C_{Dh}S_h}{\pi S_w A} = 4\frac{C_{Dh}S_h S_w}{\pi S_w b^2} = \frac{C_{Dh}d_h^2}{b^2} = C_{Dh} f_b^{-2}$$

Here we have firstly used the definition of aspect ratio, $A = b^2/S_w$, and then assumed a circular frontal area. Finally, the wing-hull ratio, $f_b = b/d_h$, defines the ratio between the wingspan, b, and hull diameter, d_h. This parameter is critical for describing the amount of lift that can be generated by the wing. The larger the ratio f_b, the more lift can be generated for a given hull design and a fixed wing aspect ratio (A). This will in turn also affect the range of achievable glide-path angles.

Parasitic drag has hull *and* wing drag components, so the assumption of $C_{Dw} \approx 0$ will lead to an underestimation of drag and overestimation of lift. Assuming a span efficiency of 1 will have a similar effect.

Substituting $u = \dot{x}/\cos\xi$ and Equation 9 into Equation 8 yields

$$\Lambda_G = \frac{4\cot^2\xi\cos\xi}{\rho\dot{x}^2\pi S_w A\left(1 - \left(1 - C_{Dh} f_b^{-2}\cot^2\xi\right)^{\frac{1}{2}}\right)} \tag{10}$$

where glide angle is subject to bounds dictated by stall. This hydrodynamic model is only accurate for small angles of attack (Graver, 2005).

3.3.1. Normalize with Respect to Ideal

After normalizing the glider transit performance (Equation 10) with respect to the ideal transit performance (Equation 3), we obtain

$$\lambda_G = \frac{C_{Dh} f_b^{-2} \cot^2 \xi \cos \xi}{2\left(1 - \left(1 - C_{Dh} f_b^{-2} \cot^2 \xi\right)^{\frac{1}{2}}\right)} \tag{11}$$

The glider transit efficiency model, Equation 11, shows that the transit efficiency of the glider is independent of horizontal velocity, and wing planform area, but dependent on glide-path angle.

3.3.2. Optimal Glide-Path Angle

In general, the optimum glide-path angle can be found as a function of the wing-hull ratio (f_b) and the hull drag coefficient (C_{Dh}). This can be used to reduce the parameter space of Equation 11. By setting $\frac{\delta \lambda_G}{\delta \xi} = 0$ and solving for ξ, we get the following equation for the optimal glide-path angle:

$$\xi_{Opt} = \pm \tan^{-1}\left(\frac{1}{3}\left(Q + 4\left(C_{Dh} f_b^{-2}\right) - 2 + \frac{20\left(C_{Dh} f_b^{-2}\right) + 16\left(C_{Dh} f_b^{-2}\right)^2 + 4}{Q}\right)^{\frac{1}{2}}\right) \tag{12}$$

where

$$Q = \left(\frac{123}{2}\left(C_{Dh} f_b^{-2}\right) + 120\left(C_{Dh} f_b^{-2}\right)^2 + 64\left(C_{Dh} f_b^{-2}\right)^3 - 8 + 18\left(-6\left(C_{Dh} f_b^{-2}\right) - \frac{183}{16}\left(C_{Dh} f_b^{-2}\right)^2 - 6\left(C_{Dh} f_b^{-2}\right)^3\right)^{\frac{1}{2}}\right)$$

This result shows that the optimal glide-path angle is independent of the vehicle's velocity. Consequently, for a given hull design, glider transit efficiency is only a function of f_b.

FIGURE 3

Glider efficiency vs. glide angle for the Slocum. The optimal glide-path angle is using the parameters specified in Table 1.

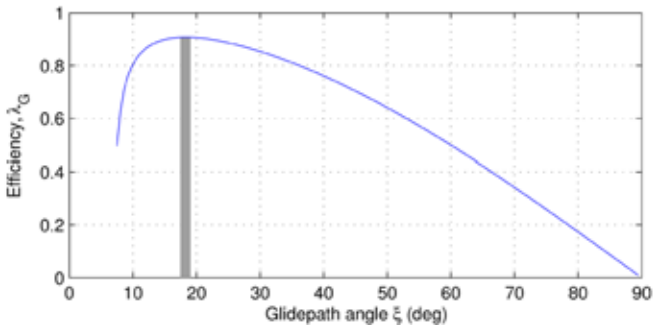

To demonstrate this relationship, Figure 3 shows the transit performance of Slocum with respect to the glide-path angle. Transit efficiency, λ_G, is maximized at a glide-path angle of 18°.

4. Results

Each model has been distilled down to one dimensionless design parameter. This reduction in parameter space allows for the direct comparison between the two propulsion methods. In this section, we explore the nuances of these models and show that it is possible to design either vehicle class to attain the same transit efficiency.

The models presented in this article are generally applicable across vehicles of the classes considered. However, in order to provide context to our work, we compare the results of two real-world, fielded vehicles—REMUS100 and Slocum. The parameters used to generate the transit performance and efficiency for REMUS100 (Allen et al., 2000) and Slocum (Sherman et al., 2001, Geisbert, 2007) are given in Table 1.

TABLE 1

Parameters for the Slocum and REMUS100 AUVs.

Parameter	Slocum	REMUS100
C_{Dh}	0.4305	0.267
$S_h(m^2)$	0.034	0.028
Design ratios	f_b = 4.8077	f_p = 0.7353

4.1. Propeller-Driven AUV

Figure 4 summarizes the transit efficiency for a propeller-driven AUV, $\lambda_{AD,}$ as a function of the propeller-hull ratio, f_p.

The transit efficiency of a propeller-driven AUV can be improved by

FIGURE 4

Efficiency of a propeller-driven AUV with varying propeller–hull ratios, f_p, for selected drag coefficients.

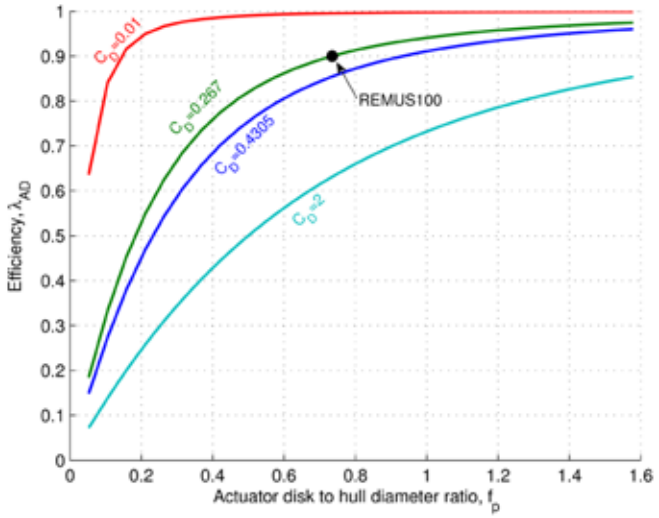

increasing its propeller–hull ratio. However, improvements to efficiency diminish as propeller–hull ratio increases, particularly at lower drag coefficients.

4.2. Glider/Buoyancy-Driven AUV

Figure 5 summarizes the transit efficiency for a glider, λ_G, as a function of the wing-hull ratio, f_b. It is evident that a larger wing–hull ratio provides higher transit efficiency, which is consistent with the results presented by Sherman et al. (2001).

Improvements to transit efficiency, however, occur at a diminishing rate and again this is particularly prevalent for low drag coefficients. Significant gains to transit efficiency obtained by increasing the wing–hull ratio are harder to achieve for lower drag designs.

Figure 6 shows how the optimal glide-path angle changes with the wing–hull ratio for selected drag coefficients. As the wing–hull ratio increases, the glide-path angle becomes shallower. Furthermore, a glider with a low coefficient of drag will transit at a relatively shallow glide-path angle.

FIGURE 5

Efficiency vs. wing–hull ratio for selected drag coefficients.

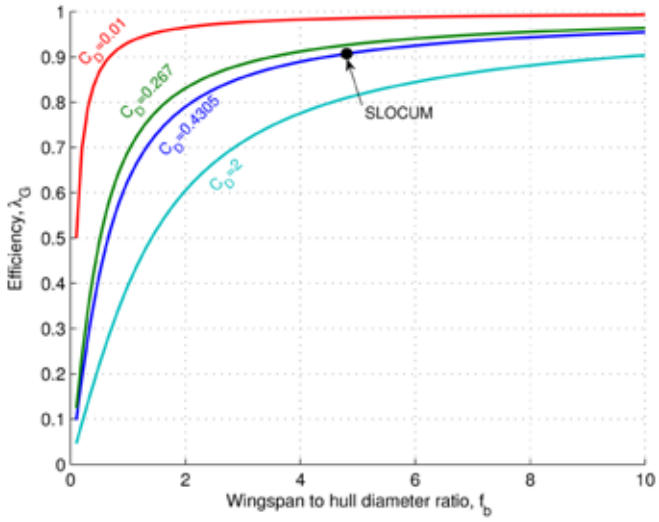

The glider model derived in this article implies that transit efficiency is independent of aspect ratio, A. This is also true for transit performance because the $S_w A$ term in the denominator of Equation 10 is equivalent to wingspan squared (b^2). As a result, the parameter f_b does not fully specify the shape of the wing. According to our analysis, a glider with a low aspect ratio (wide wing) will have an equivalent transit efficiency to a glider with a high aspect ratio (slender wing) of the same wingspan and hull design (see Figure 7). Because the effects of parasitic wing drag are omitted from the model, there is no penalty associated with large wing planform area for a given wing–hull ratio.

The relationship between angle of attack, α, and aspect ratio, A, given by Equation 9 is depicted in Figure 8. Our model allows for both low aspect (wide) and high aspect (slender) ratio wings to have the same transit efficiency. However, Figure 8 shows that our model is detailed enough to capture the requirement of these designs to operate at different angles of attack. From a design perspective, it is desirable to maximize the aspect ratio for a given wingspan to minimize parasitic drag, subject to structural and stall constraints (Sherman et al., 2001). This produces a wing geometry resembling that of sailplanes.

4.3. Comparison of Transit Performance

The vehicle design parameters f_p and f_b can be varied so that a propeller-driven AUV and a glider have the same

FIGURE 6

Optimal glide-path angle vs. wing–hull ratio for selected drag coefficients.

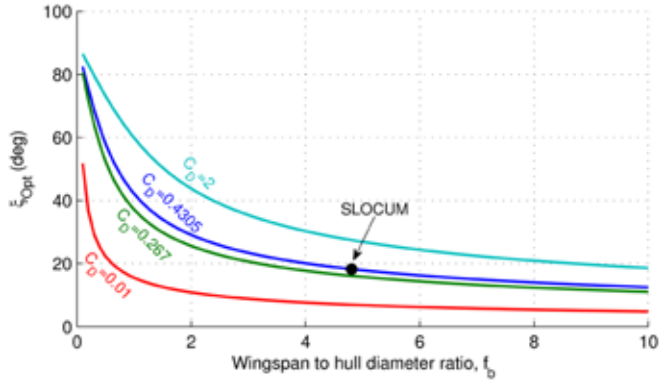

transit efficiency. The exact relation between these design parameters can be found by equating the transit efficiencies given by Equation 4 and Equation 11 to yield

$$f_p = \frac{C_{Dh}^{\frac{1}{2}}}{\sqrt{\left(\frac{4\left(1-\sqrt{1-C_{Dh} f_b^{-2} \cot^2 \xi_{Opt}}\right)}{C_{Dh} f_b^{-2} \cot^2 \xi_{Opt} \cos \xi_{Opt}} - 1\right)^2 - 1}} \tag{13}$$

Equation 13 states propeller–hull ratio as a function of wing–hull ratio and hull drag coefficient (where $\xi_{opt} = f(f_b, C_{Dh})$). This relation specifies an equally efficient propeller-driven AUV configuration for a given glider configuration.

Figure 9 is a graphical representation of the relationship derived in Equation 13 for a range of drag coefficients and design parameters. The solid curves represent equivalent transit efficiencies for a constant drag coefficient. A point on these curves provides the design parameters f_p and f_b that will produce the same transit efficiency for a given drag coefficient. The dotted lines show constant transit efficiency across all drag coefficients.

FIGURE 7

Gliders with equivalent wingspan and hull designs but different aspect ratio. On the left is a high aspect ratio wing and on the right is a low aspect ratio wing. According to our model, these designs have the same transit efficiency but different steady-state glide-path angles when transiting optimally.

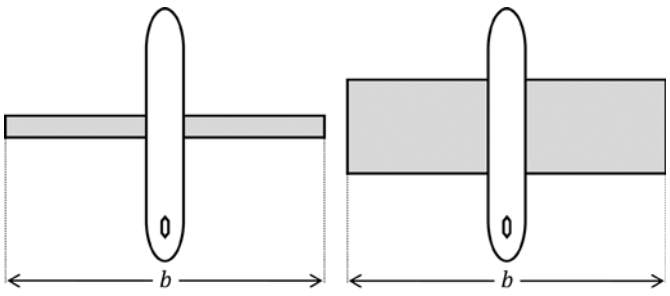

For the ranges of drag considered, Figure 9 shows that the wing–hull ratio has to be increased proportionally more than the propeller–hull ratio to achieve the same gain in transit efficiency. This effect is greater for low drag coefficients. For the purpose of relating this general result to realistic designs, the positions of REMUS100 and Slocum have been highlighted on the plot. This plot shows that REMUS100 and Slocum have similar transit efficiencies in their original configurations, according to our models.

Table 2 shows the parameters for propeller-driven AUVs and gliders with transit efficiencies equal to REMUS100 (90%), Slocum (91%), and a notional high-performance vehicle having a transit efficiency of 95%. Recall that additional losses in the system, such as mechanical and electrical losses, are not included in our definition of transit efficiency.

The REMUS100 and Slocum vehicles have very similar transit efficiencies (Table 2). This similarity can be attributed to their similar hull designs and the fact that transit efficiency is independent of horizontal velocity as per Equations 4 and 11. The difference in their endurances is due to their different velocity regimes and hotel loads. According to our analysis, each vehicle could exhibit equivalent transit efficiencies with minimal modifications. For example, REMUS100 would need a propeller-hull ratio of $f_p \approx 0.77$ to attain an equivalent transit efficiency to Slocum (Prop-AUV1 in Table 2). This implies a propeller diameter of approximately 14.6 cm instead of its standard propeller diameter of 14 cm (Allen et al., 2000). Conversely, for Slocum to exhibit the same efficiency as REMUS100 (Glider-AUV1 in Table 2), it would require a span ratio

FIGURE 8

Angle of attack vs. aspect ratio for selected wing–hull ratios. The Slocum drag coefficient from Table 1 is used.

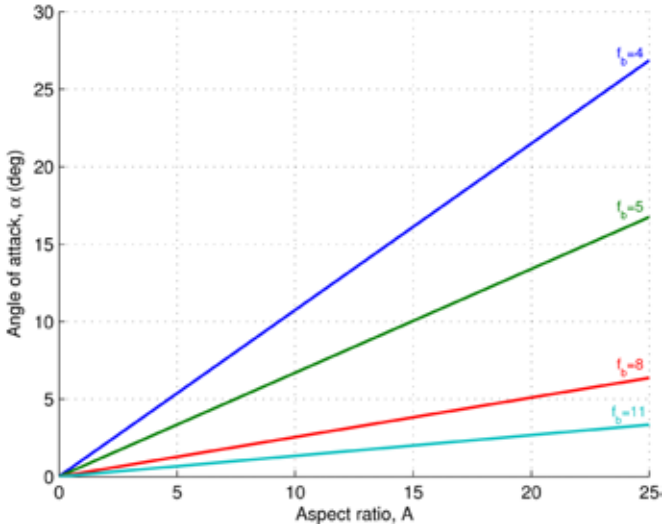

FIGURE 9

Span ratio, f_b, vs. propeller–hull ratio, f_p, for equal transit efficiency. Points for the Slocum glider and the REMUS100 AUV have been shown.

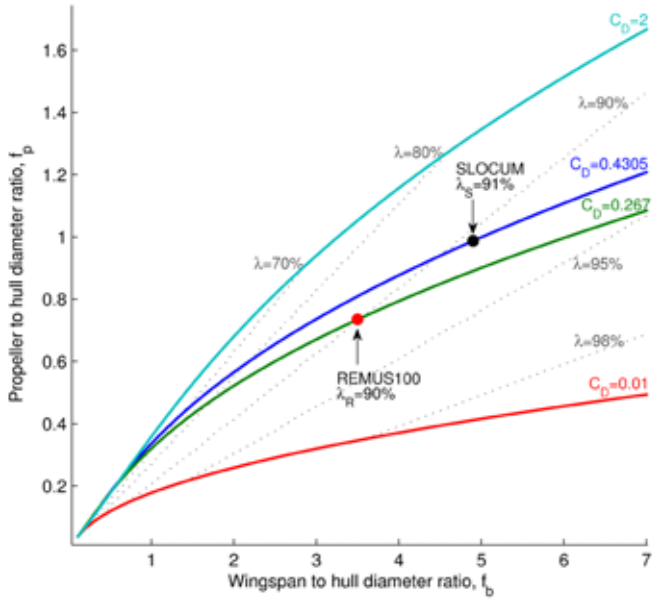

of about 4.5 rather than its current value of approximately 5, implying a decrease in wingspan from about 1 m to 0.94 m.

To reach a transit efficiency of 95%, REMUS100 (Prop-AUV2, Table 2) would require a propeller diameter of d_p = 21.0 cm, which is an increase of 50% on the standard propeller size. For Slocum to reach a transit efficiency of 95% (Glider-AUV2, Table 2), a wingspan of about 1.9 m would be required. This represents an increase of over 85% on the original wingspan.

This case study shows that the wing-hull ratio of Slocum has to be increased proportionally more than the propeller-hull ratio of REMUS100 to achieve the same gain in transit efficiency. It is important to note that the REMUS100 and Slocum have different drag coefficients. However, within the range of coefficients considered, the relationship holds.

5. Conclusion

We have shown that both methods of propulsion can be designed to achieve the same transit efficiency using a first-principle analysis. These results imply that neither propeller-driven AUVs nor gliders have any advantage over the other with respect to transit efficiency. For example, the long endurance of a glider may be achieved by a similarly sized propeller-driven vehicle designed to transit slowly. The choice of propulsion method should be driven exclusively by the application and operational requirements, regardless of velocity or hotel load.

Given that no platform offers superior transit performance, there are no optimal characteristics to combine. This outcome can be extended to hybrid vehicles—a system that attempts to incorporate a buoyancy engine, wings, and thrusters will require more volume for hardware, reducing energy storage capacity for no realizable advantage in transit performance.

Our results need to be viewed in light of the assumptions we have made. By excluding the effect of parasitic drag, no penalty is paid for the surface areas of the wings and propeller blades. Including the effects of parasitic drag introduces a Reynolds number dependence that may further differentiate one platform from another in terms of transit efficiency when operating in a low velocity regime. However,

TABLE 2

Summary of selected points from Figure 9.

Vehicle	λ	C_{Dh}	d_h	Design Parameter	Dimensional Parameter
REMUS100	90%	0.267	19 cm	f_p = 0.7353	d_p = 14.0 cm
Prop-AUV1	91%	0.267	19 cm	f_p = 0.769	d_p = 14.6 cm
Prop-AUV2	95%	0.267	19 cm	f_p = 1.104	d_p = 21.0 cm
Glider-AUV1	90%	0.4305	20.8 cm	f_b = 4.5	b = 0.94 m
Slocum	91%	0.4305	20.8 cm	f_b = 4.9	b = 1.02 m
Glider-AUV2	95%	0.4305	20.8 cm	f_b = 9.1	b = 1.89 m

including higher order effects, such as parasitic drag and design-specific mechanical losses, introduces complexities into the vehicle models that make it difficult to draw fair and general comparisons between the propulsion modes.

Acknowledgments

This work is supported by the Australian Research Council (ARC) Center of Excellence program and funded by the New South Wales State Government.

Lead Authors:

Daniel Steinberg
Asher Bender
Ariell Friedman
Australian Centre for Field Robotics
School of Aerospace Mechanical and Mechatronic Engineering
University of Sydney
Email: d.steinberg@acfr.usyd.edu.au; a.bender@acfr.usyd.edu.au; a.friedman@acfr.usyd.edu.au

References

Allen, B., Vorus, W.S., Prestero, T. 2000. Propulsion system performance enhancements on REMUS AUVs. OCEANS 2000 MTS/IEEE Conf Exhib. 3(3):1869-1873.

Bradley, A.M., Feezor, M.D., Singh, H., Sorrell, F.Y. 2001. Power systems for autonomous underwater vehicles. IEEE J Oceanic Eng. 26(4):526-38.

Carlton, J. 2007. Marine Propellers and Propulsion. Oxford: Elsevier Butterworth-Heinemann.

Davis, R.E., Eriksen, C., Jones, C.P. 2002. Autonomous Buoyancy-Driven Underwater Gliders. In: The Technology and Applications of Autonomous Underwater Vehicles, ed. G. Griffiths, 37-58. London: Taylor and Francis.

Electric glider. Available from http://www.webbresearch.com/electricglider.aspx (accessed April 1, 2009).

Furlong, M.E., McPhail, S.D., Stevenson, P. 2007. A concept design for an ultra-long-range survey class AUV. In: OCEANS 2007. pp. 1-6. Aberdeen: IEEE.

Geisbert, J.S. 2007. Hydrodynamic modelling for autonomous underwater vehicles using computational and semi-empirical methods. Masters thesis, Virginia Polytech Institute and State University. 99 pp.

Graver, J.G. 2005. Underwater gliders: Dynamics, control and design. Ph.D. thesis, Princeton University. 292 pp.

Griffiths, G., Davis, R., Eriksen, C., Frye, D., Marchand, P., Dickey, T., Weller, R. 2001. Towards New platform technology for sustained observations. In: Observing the Ocean For Climate In The 21st Century, ed. Koblinsky C.J., Smith N.R., 324-337. Melbourne: Bureau of Meteorology.

Griffiths, G., Merckelbach, L., Smeed, D. 2007. On the performance of three deep-diving underwater gliders. In: OCEANS 2007. pp. 1-5. Aberdeen: IEEE.

Jenkins, S.A., Humphreys, D.E., Sherman, J., Osse, J., Jones, C., Leonard, N., Graver, J., Bachmayer, R., Clem, T., Carroll, P., Davis, P., Berry, J., Worley, P., Wasyl, J. 2003. Underwater glider system study. Scripps Institution of Oceanography Technical Report. 242 pp.

REMUS100 specification. Available from http://www.hydroidinc.com/100spec.html (accessed March 29, 2009).

Roskam, J. 2008. Airplane Design: Part VI. Preliminary Calculation of Aerodynamic, Thrust and Power Characteristics, Vol. 6. Kansas: DARcorporation. 550 pp.

Schofield, O., Kohut, J., Roarty, H., Glenn, S., Jones, C., Webb, D. 2008. Enabling discovery based science with webb gliders. In: US/EU-Baltic International Symposium, IEEE/OES. pp 1-6. Tallinn: IEEE.

Sherman, J., Davis, R.E., Owens, W.B., Valdes, J. 2001. The autonomous underwater glider 'Spray'. IEEE J Oceanic Eng. 26(4):437-446.

Steinberg, D., Bender, A., Friedman, A. 2009. Toward selection of a propulsion method for a long range benthic imaging AUV. In: International Symposium on Unmanned Untethered Submersible Technology (UUST). University of New Hampshire, Autonomous Undersea Systems Institute.